

# DeepIPC: Deeply Integrated Perception and Control for an Autonomous Vehicle in Real Environments<sup>★</sup>

Oskar Natan<sup>a,b,\*</sup>, Jun Miura<sup>a</sup>

<sup>a</sup>*Department of Computer Science and Engineering, Toyohashi University of Technology, 1-1 Hibarigaoka, Tempaku-cho, Toyohashi, 441-8580, Aichi, Japan*

<sup>b</sup>*Department of Computer Science and Electronics, Gadjah Mada University, Bulaksumur, Caturtunggal, Sleman, 55281, Yogyakarta, Indonesia*

## Abstract

We propose DeepIPC, an end-to-end autonomous driving model that handles both perception and control tasks in driving a vehicle. The model consists of two main parts, perception and controller modules. The perception module takes an RGBD image to perform semantic segmentation and bird's eye view (BEV) semantic mapping along with providing their encoded features. Meanwhile, the controller module processes these features with the measurement of GNSS locations and angular speed to estimate waypoints that come with latent features. Then, two different agents are used to translate waypoints and latent features into a set of navigational controls to drive the vehicle. The model is evaluated by predicting driving records and performing automated driving under various conditions in real environments. The experimental results show that DeepIPC achieves the best drivability and multi-task performance even with fewer parameters compared to the other models. Codes will be published at <https://github.com/oskarnatan/DeepIPC>.

**Keywords:**

Perception-action integration, sensor fusion, end-to-end imitation learning, autonomous driving

## 1. Introduction

End-to-end learning has become a preferable approach in autonomous driving as manual configuration to integrate task-specific modules is no longer needed. This technique allows the model to share useful features directly from perception modules to controller modules. Moreover, the model can learn and receive extra supervision from a multi-task loss function that considers several performance criteria. All these benefits result in a better model performance even with a smaller model size due to its compactness [1][2]. To date, there have been a lot of works in the field of end-to-end autonomous driv-

ing, whether it is based on simulation [3], or offline real-world where the model predicts a set of driving records [4], or online real-world where the model is deployed for automated driving [5]. Besides dealing with diverse conditions such as driving on a sunny day or low-light evening, another challenge that remains in online real-world autonomous driving is that the model must deal with noise and inaccuracy of sensor measurement. This issue needs to be addressed as it affects model performance [6][7].

To address those challenges, some works have been conducted with a focus on simulation-to-real adaptation. Although the models still suffer from performance losses due to sensor inaccuracies and diverse conditions in real environments, these approaches are said to be promising for future autonomous driving [8][9]. On the other hand, some different approaches have been proposed with a focus on end-to-end imitation learning where the

<sup>★</sup>Supplementary video: <https://youtu.be/AiKotQ-lAzw>

<sup>\*</sup>Corresponding author

Email addresses: [oskar.natan.ao@tut.jp](mailto:oskar.natan.ao@tut.jp);  
[oskarnatan@ugm.ac.id](mailto:oskarnatan@ugm.ac.id) (Oskar Natan),  
[jun.miura@tut.jp](mailto:jun.miura@tut.jp) (Jun Miura)

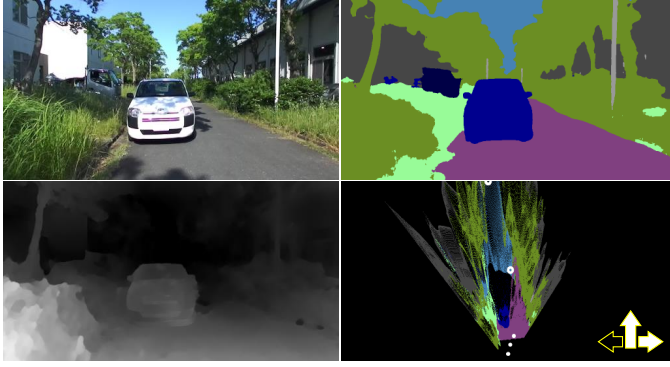


Figure 1: DeepIPC perceives the environment by performing segmentation and BEV semantic mapping. Simultaneously, it estimates waypoints and controls to drive the vehicle. The detailed architecture of DeepIPC can be seen in Fig. 2.

model is trained to mimic an expert driver in dealing with complicated situations on the street [10][11]. These approaches are preferred as they are easier and can be done with a simple supervised learning technique [12]. Moreover, plenty of publicly available datasets along with self-made datasets can be used to train the model to enrich its driving experiences. Considering its advantage, we adopt this approach and propose a model namely DeepIPC (Deeply Integrated Perception and Control). The architecture of DeepIPC is based on our previous work [1] with some improvements to deal with the issues.

Concisely, DeepIPC is a model that can be forced to learn how to compensate for noise and inaccuracy of sensor measurement implicitly by mimicking expert behavior to achieve human-like autonomous driving [13][14]. DeepIPC processes multi-modal data that contain several quantities needed to perceive the environment and drive the vehicle in one forward pass. The perception parts take an RGBD image to perform semantic segmentation and BEV semantic mapping. Simultaneously, the controller parts estimate waypoints and navigational controls based on the extracted perception features, wheel’s angular speeds, and route points. Unlike in an ideal simulated environment, DeepIPC must deal with real implementation issues. For example, it must compensate for the issue of inaccurate route points positioning caused by the inaccuracy of the GNSS receiver and IMU sensor. Then, there are also plenty of noises on the RGBD camera that affect the scene understanding capability. As shown in Fig. 1, DeepIPC must be able to safely avoid the obstacle by predict-

ing navigational controls and waypoints correctly in the traversable area although the given route points (two white circles on the bottom-right image) are not located accurately in the local coordinate. Hence, we state the novelties as follows:

- We propose DeepIPC, an improved version of our previous model [1] for driving a robotic vehicle in real environments. Concisely, the perception parts are modified to process a wider RGBD image for better perception. Then, the controller parts are enhanced with an updated control policy to allow a higher degree of maneuverability. Moreover, it is also fed with two route points and wheel’s angular speeds for better driving intuition.
- As we demonstrate the real-world experiments of our previous study on simulation-based autonomous driving [1], we exhibit how a proof-of-concept study can be realized by addressing some implementation issues. Furthermore, unlike many studies that only predict driving records, we deploy DeepIPC to perform real-world automated driving. This also exposes the usefulness of end-to-end imitation learning, not only for a simple model but also for a complex multi-input multi-output model.
- We compare DeepIPC with other models to get a clearer performance justification. All models are evaluated by predicting a set of driving records and performing real-world automated driving under different conditions. Then, we also define a new metric to evaluate the model performance based on the number of driver interventions and not by the number of collisions. This is necessary to avoid any damage to the vehicle. The experimental results show that DeepIPC achieves the best performance even with fewer parameters. This establishes the effectiveness of our network architecture.

## 2. Related Works

In this section, we review some related works that focus on end-to-end autonomous driving. Then, we point out the key ideas which inspire our work and as an objective for comparative study.

### 2.1. Perception-Action Coupling

Among various approaches in the field of autonomous driving, perception has always been the first stage as it is important to understand the surrounding area before planning and action. It can be achieved by performing various vision tasks such as semantic segmentation, depth estimation, and object detection [15][16][17]. In the autonomous driving area, Hahner et al. proposed a segmentation model that is made specifically to deal with foggy conditions [18]. Then, different work is proposed by Rajaram et al. [19] where a model called RefineNet is used to perform object detection. Besides completing a single vision task, the model can be pushed further to perform multiple vision tasks simultaneously to achieve a better scene understanding [20].

After achieving the ability to perceive the environment, a model also needs to leverage this ability to support the controller parts. In the field of end-to-end autonomous driving where perception and control are coupled together, better visual perception means better drivability as the controller gets better features directly from the perception module [21]. The work in coupling perception and control modules has been done by Ishihara et al. [22] where an end-to-end model is deployed to perform multiple vision tasks and predict navigational controls at the same time. Similar work is also proposed by Chitta et al. [23] where a model called AIM-MT (auto-regressive image-based model with multi-task supervision) completes perception and control tasks simultaneously to drive a vehicle. It is disclosed that performing vision tasks can improve drivability as the controller receives better perception features.

Similar to Ishihara et al. [22] and Chitta et al. [23], the perception parts of DeepIPC are guided by completing a vision task to provide better features. However, it only uses semantic segmentation as auxiliary supervision since the depth is considered as an input. For a comparative study, we use AIM-MT as a representative of the model that uses depth estimation as an extra supervision in providing better features.

### 2.2. Multi-modal Fusion

Processing one kind of data modality is not reliable for autonomous driving as it can be failed under certain conditions. Therefore, more heterogeneous

data is needed to cover each other's weaknesses and produce more meaningful information through sensor fusion techniques [24][25]. Some studies have been conducted in the field of sensor fusion for autonomous driving. To be more specific in the camera-LiDAR fusion, Prakash et al. [26] have proposed a model that processes RGB images and point clouds to perceive the environment and drive the vehicle. A certain transformer-based module called TransFuser [27] is used to learn the relation between RGB images and point clouds to achieve better perception. Then, another work is proposed by Niesen and Unnikrishnan [28] where camera and radar are fused to achieve accurate 3D depth reconstruction.

Mounting two different sensors can be another issue as more space, equipment, and extra budgets are needed. Therefore, using an equivalent sensor that is cheaper and can do a similar function may be preferable to tackle this problem. For example, a LiDAR can be replaced with a depth camera (merged with an RGB camera) to perceive the depth [29]. In the use of RGBD image for autonomous driving, Huang et al. [30] demonstrated how RGB image and depth map can be fused and extracted from the early perception stage to provide better features for the controller. Besides pixel-to-pixel fusion, the depth map can be also projected to produce a BEV semantic map [1]. Thus, the model can perceive from the top-view perspective for a better perception.

Together with AIM-MT [23], we deploy Huang et al.'s model [30] for a comparative study with the objective of comparing the performance of different sensor fusion strategies. Huang et al. fuse the information by processing RGB and depth at the early stage to extract a deeper relation on each pixel. Meanwhile, DeepIPC fuses the information by performing BEV semantic mapping to get the advantage of perceiving from a different perspective.

### 2.3. Real-world Imitation Learning

In order to achieve end-to-end autonomous driving, one approach is to proceed with behavior cloning or imitation learning strategies which can be done easily in a supervised learning manner. By using the end-to-end imitation learning strategy, we can create a single deep learning model to imitate the behavior of an expert driver in manipulating naviga-

tional controls or effectors for handling complicated situations on the street [31][32]. This can be derived from publicly available datasets or simulated with a simulator to enrich the model’s driving experiences [33][34]. Therefore, the model will be able to perform human-like autonomous driving [35].

Imitation learning has been widely used for real-world experiments. In the application to mobile robotics and autonomous vehicles, Cai et al. [36] propose a vision-based model for driving a toy-size autonomous race car in a fixed circuit. This work shows how the imitation learning technique can be used to train a simple model to learn the mapping function between an RGB image as the input and navigational controls as the outputs. Not only simple models, but this technique is also applicable to multi-input multi-output models that process multiple data. Recent work by Chatty et al. [37] demonstrates the use case of imitation learning for cognitive map building used for navigating a mobile robot. Then, Hoshino et al. [38] also use the imitation-based end-to-end multi-task learning technique for motion planning and controlling a mobile robot in a challenging environment. Another similar work is proposed by Yan et al. [39] where an end-to-end model is used to control a robotic shark. Although these methods look promising, imitation learning sometimes causes an issue of generalization ability in new environments.

Following the success of these works in using imitation learning for complex multi-input multi-output models, we also use this approach to train DeepIPC for driving a robotic vehicle in real environments. Then, to overcome the generalization ability problem, we employ two control agents to manipulate the vehicle’s end-effectors. As there are more decision-makers in its architecture, DeepIPC will be able to consider different aspects of drivability.

### 3. Methodology

In this section, we explain the model architecture and its improvement in detail. Then, we describe the dataset used for imitation learning. We also describe the training setup and define several formulas used to supervise the model. Finally, we explain the evaluation setting including the metrics used to justify the model performance.

#### 3.1. Proposed Model

As mentioned in Section 1, the architecture of DeepIPC is based on our previous work [1] that is composed of perception and controller. As shown in Fig. 2, the perception phase begins with semantic segmentation on RGB image with a standard encoder-decoder network enhanced with several skip connections [40][41]. The RGB encoder is made of a pretrained Efficient Net B3 [42] while the decoder is composed of multiple convolution blocks where each block consists of ( $2 \times (3 \times 3$  convolution + batch normalization [43] + ReLU [44]) + bilinear interpolation) and a pointwise  $1 \times 1$  convolution followed with sigmoid activation. Furthermore, we generate point clouds from the depth map and make projections with the predicted segmentation map to obtain a BEV semantic map with a coverage area of 24 meters to the front, left, and right from the vehicle location. Thus, the vehicle is always positioned at the bottom center of the BEV semantic map. Then, the BEV semantic map is encoded by an Efficient Net B1 encoder [42] to obtain its features. With this configuration, DeepIPC has both front and top perspectives to perceive the surrounding area.

In the controller module, both RGB and BEV semantic features are processed by a fusion block module which is composed of pointwise ( $1 \times 1$ ) convolution, global average pooling, and linear layer. This module is responsible for learning the relation between features from the front and top-view perspectives and resulting in more compact latent features. Then, a gated recurrent unit (GRU) [45] is used to decode the latent features based on the measurement of the left and right wheel’s angular speeds, predicted waypoints, and two route points that have been transformed into local BEV coordinates. The decoded features are processed further by a linear layer to predict  $\Delta x$  and  $\Delta y$ . Thus, the next waypoint coordinate can be calculated with (1).

$$x_{i+1}, y_{i+1} = (x_i + \Delta x), (y_i + \Delta y) \quad (1)$$

To be noted, the waypoints prediction process is looped over three times as there are three waypoints to be predicted. In the first loop, the waypoint is initialized with the vehicle position in the local BEV coordinate which is always at (0,0). In the end, the waypoints are translated into a set of naviga-

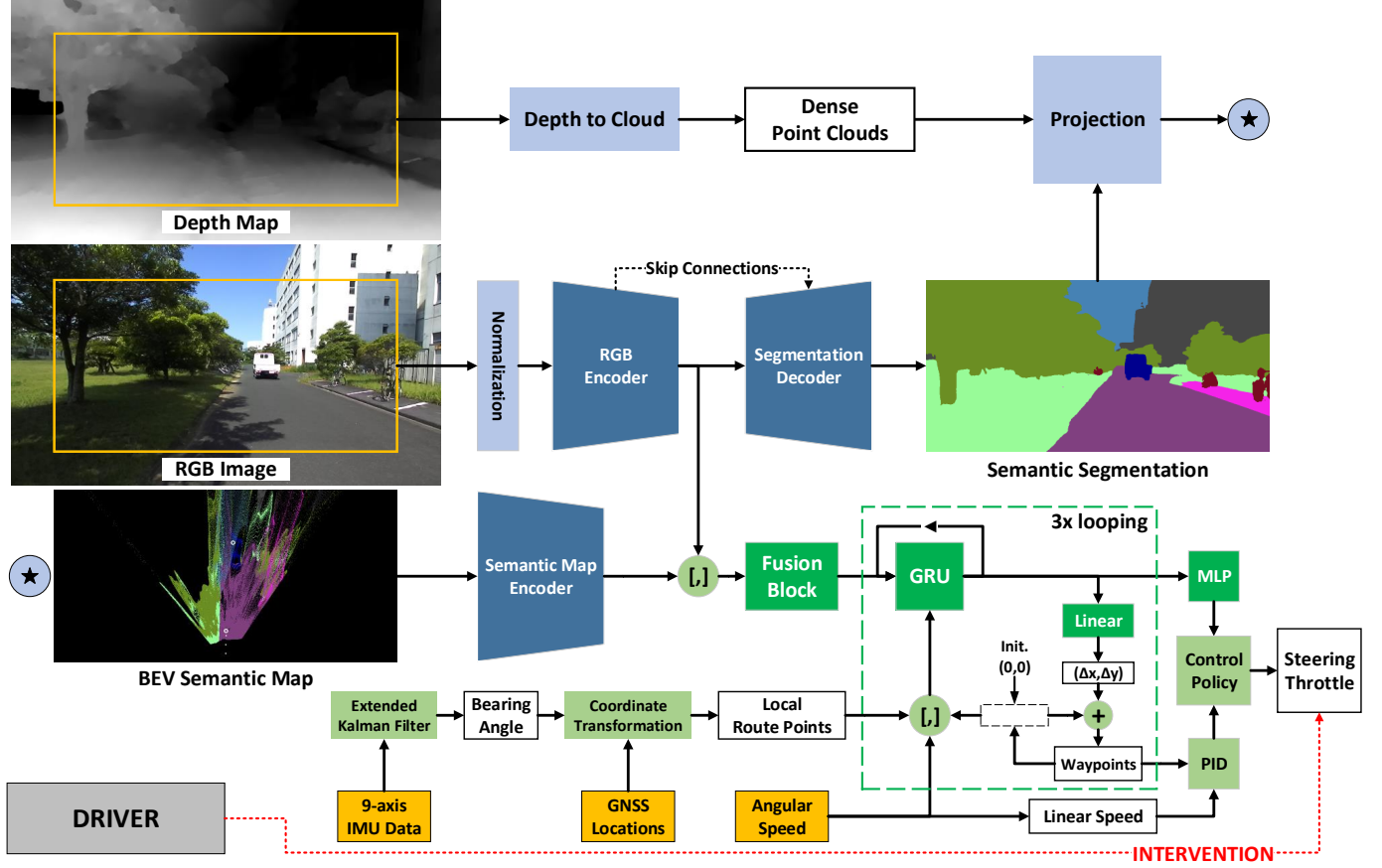


Figure 2: The architecture of DeepIPC. Blue blocks are parts of the perception module, while green blocks are parts of the controller module. Light-colored blocks are not trainable, while the darker ones are trainable. In the BEV semantic map, waypoints are denoted with white dots, while route points are denoted with white circles.

tional controls (steering and throttle) by two PID controllers in which their  $K_p, K_i, K_d$  parameters are tuned empirically. The final features used to predict the last waypoint are also processed by a multi-layer perceptron (MLP) block to estimate the navigational controls directly. The final action that actually drives the vehicle is made by a control policy that combines both PID and MLP controls as shown in Algorithm 1. We set a threshold of 0.1 as the minimum steering and throttle level for an agent to be able to drive the vehicle. This mechanism allows an agent to take control completely over the other agent and results in better maneuverability.

### 3.2. Model Improvement

Different from our previous work [1], the model is modified to improve its performance and deal with real-world implementation issues. First, as the input to the perception module, we consider a wider ROI of  $H \times W = 512 \times 1024$  at the center of the RGBD image.

Then, they are resized to  $H \times W = 256 \times 512$  to reduce the computational load. With a wider input resolution, the model is expected to have a better scene understanding capability. Second, as the input to the controller module, we feed the left and right wheel’s angular speeds for better turning as the speed will be different on each wheel. Third, two route points are given instead of one route point at a time. Relying only on one route point is very risky due to the possibility of mislocation caused by GNSS and IMU inaccuracies that affect the global-to-local coordinate transformation. If the route point is mislocated, the model will likely fail to predict waypoints and navigational controls correctly. Besides that, giving two route points will give the model a better intuition in deciding whether the vehicle should drive straight or turn depending on the location of the route points. Fourth, we also modify the control policy by allowing an agent to take the steering control completely over the other agent for better maneuverability.



---

**Algorithm 1: Control Policy**

---

$\Theta = \frac{Wp_1 + Wp_2}{2}; \theta = \tan^{-1} \left( \frac{\Theta[1]}{\Theta[0]} \right)$   
 $\gamma = 1.75 \times \|Wp_1 - Wp_2\|_F; \nu = \frac{(\omega_l + \omega_r)}{2} \times r$   
 $\mathbf{PID}_{ST} = \mathbf{PID}^{Lat}(\theta - 90)$   
 $\mathbf{PID}_{TH} = \mathbf{PID}^{Lon}(\gamma - \nu)$   
**if**  $\mathbf{MLP}_{TH} \geq 0.1$  **and**  $\mathbf{PID}_{TH} \geq 0.1$  **then**  
    **if**  $|\mathbf{MLP}_{ST}| \geq 0.1$  **and**  $|\mathbf{PID}_{ST}| < 0.1$  **then**  
        steering =  $\mathbf{MLP}_{ST}$   
    **if**  $|\mathbf{MLP}_{ST}| < 0.1$  **and**  $|\mathbf{PID}_{ST}| \geq 0.1$  **then**  
        steering =  $\mathbf{PID}_{ST}$   
    **else**  
        steering =  $\beta_{00}\mathbf{MLP}_{ST} + \beta_{10}\mathbf{PID}_{ST}$   
    throttle =  $\beta_{01}\mathbf{MLP}_{TH} + \beta_{11}\mathbf{PID}_{TH}$   
**else if**  $\mathbf{MLP}_{TH} \geq 0.1$  **and**  $\mathbf{PID}_{TH} < 0.1$  **then**  
    steering =  $\mathbf{MLP}_{ST}$ ; throttle =  $\mathbf{MLP}_{TH}$   
**else if**  $\mathbf{MLP}_{TH} < 0.1$  **and**  $\mathbf{PID}_{TH} \geq 0.1$  **then**  
    steering =  $\mathbf{PID}_{ST}$ ; throttle =  $\mathbf{PID}_{TH}$   
**else**  
    steering = 0; throttle = 0  
.....  
 $Wp_{\{1,2\}}$ : first and second predicted waypoints  
 $\mathbf{MLP}_{\{ST,TH\}}$ : steering and throttle estimated by MLP  
 $\omega_{\{l,r\}}$ : left/right angular speed  
 $r$ : vehicle's wheel radius, 0.15 m  
 $\Theta$ : aim point, a middle point between  $Wp_1$  and  $Wp_2$   
 $\theta$ : heading angle derived from the aim point  $\Theta$   
 $\gamma$ : desired speed, Frobenius norm of  $Wp_1$  and  $Wp_2$   
 $\nu$ : linear speed, average of  $\omega_l$  and  $\omega_r$  multiplied by  $r$   
 $\beta \in \{0, \dots, 1\}^{2 \times 2}$  is a set of control weights:  
 $\beta_{00} = \frac{\alpha_2}{\alpha_2 + \alpha_1}; \beta_{10} = 1 - \beta_{00}; \beta_{01} = \frac{\alpha_3}{\alpha_3 + \alpha_1}; \beta_{11} = 1 - \beta_{01}$   
where  $\alpha_1, \alpha_2, \alpha_3$  are loss weights computed by MGN algorithm [46] (see Subsection 3.4 for more details)

---

In this research, we feed the model with data from the GNSS receiver and 9-axis IMU sensor to measure several quantities needed to perform global-to-local coordinate transformation precisely. To get the local BEV coordinate for each route point  $i$ , the relative distance  $\Delta x_i$  and  $\Delta y_i$  between vehicle location  $Ro$  and route point location  $Rp_i$  must be known. The distance can be estimated from the global longitude-latitude with (2) and (3).

$$\Delta x_i = (Rp_i^{Lon} - Ro^{Lon}) \times \frac{C_e \times \cos(Ro^{Lat})}{360}, \quad (2)$$

$$\Delta y_i = (Rp_i^{Lat} - Ro^{Lat}) \times \frac{C_m}{360}, \quad (3)$$



Figure 3: The experiment area. White circles are an example of a route that consists of start, finish, and route points. (<https://goo.gl/maps/9rXobdhP3VYdjXn48>)

where  $C_e$  and  $C_m$  are earth's equatorial and meridional circumferences which are around 40,075 and 40,008 kilometers, respectively. Then, the route point coordinates  $Rp_i^{(x,y)}$  can be obtained by applying a rotation matrix as in (4).

$$\begin{bmatrix} Rp_i^x \\ Rp_i^y \end{bmatrix} = \begin{bmatrix} \cos(\theta_{ro}) & -\sin(\theta_{ro}) \\ \sin(\theta_{ro}) & \cos(\theta_{ro}) \end{bmatrix}^T \begin{bmatrix} \Delta x_i \\ \Delta y_i \end{bmatrix}, \quad (4)$$

where  $\theta_{ro}$  is the vehicle's absolute orientation to the north pole (bearing angle). It is estimated by a 9-axis IMU sensor's built-in function based on Kalman filtering on 3-axial acceleration, angular speed, and magnetic field. The global-to-local route points transformation may not be so accurate due to sensor inaccuracy or noisy measurement. Hence, the model is forced implicitly to learn how to compensate for this issue by mimicking expert behavior for estimating the waypoints and navigational controls.

### 3.3. Dataset

In imitation learning, a considerable amount of expert driving records is needed for training and validation (train-val) [47][48][49]. To create the dataset, we drive the vehicle at a speed of 1.25 m/s in a certain area inside Toyohashi University of Technology, Japan. As shown in Fig. 3, the left region is used for the train-val, and the right region is used for the test. We consider two experiment conditions which are noon and evening. For each condition, we record the driving data one time for the train-val and three times for the test. There are 12 routes in the train-val region and 6 routes in the test region. Each route is composed of several route points with a gap of 12 meters

Table 1: Dataset Information

Conditions	Noon and evening
Total routes	12 (train-val) and 6 (test)
$\mathcal{N}$ samples*	10151 (train), 9679 (val), 18975 (test)
Devices	WHILL C2 vehicle (+rotary) Stereolabs Zed RGBD camera U-blox Zed-F9P GNSS receiver Witmotion HWT905 IMU sensor
Object classes	None, road, sidewalk, building, wall, fence, pole, traffic light, traffic sign, vegetation, terrain, sky, person, rider, car, truck, bus, train, motorcycle, bicycle

\* $\mathcal{N}$  samples is the number of observation sets. Each set consists of an RGBD image, GNSS location, 9-axis IMU measurement, wheel’s angular speed, and the level of steering and throttle.

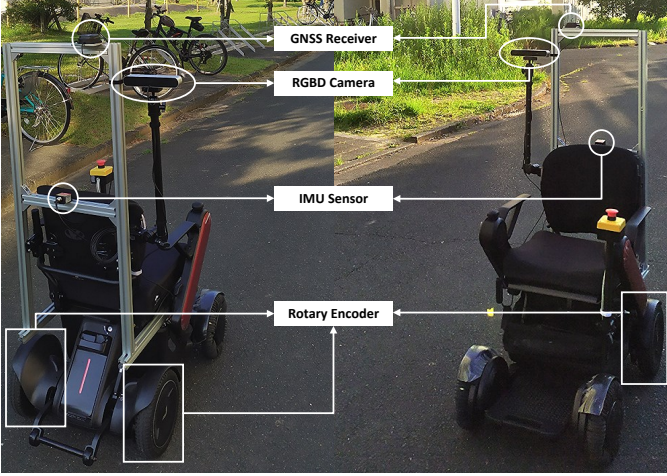


Figure 4: Sensor placement on a robotic vehicle. The rotary encoder is mounted inside each rear wheel.

between each other. The route point will be changed once the vehicle is 4 meters close. In completing the point-to-point navigation task, the model must follow the route points in driving the vehicle. The observation is recorded at 4 Hz where one observation set consists of an RGBD image, GNSS location, 9-axis IMU measurement, wheel’s angular speed, and the level of steering and throttle. The devices used to retrieve the data are mentioned in Table 1, while their placement can be seen in Fig. 4.

As mentioned in Subsection 3.1, DeepIPC predicts waypoints, navigational controls, and semantic segmentation maps. As for waypoints ground truth, we leverage the vehicle’s trajectory where the vehicle’s location in one second, two seconds, and three seconds in the future are considered as the waypoints to be predicted. Meanwhile, navigational controls ground truth can be obtained from the record of steering and throttle levels. To avoid time-consuming manual annotation, we use SegFormer [50] pre-trained on the Cityscapes dataset [51] to provide pseudo-labels by performing semantic segmentation on all RGB images in twenty different classes as mentioned in Table 1.

### 3.4. Training

With using the multi-task learning paradigm, DeepIPC can be supervised by a combination of weighted loss functions as in (5).

$$\mathcal{L}_{MTL} = \alpha_0 \mathcal{L}_{SEG} + \alpha_1 \mathcal{L}_{WP} + \alpha_2 \mathcal{L}_{ST} + \alpha_3 \mathcal{L}_{TH}, \quad (5)$$

where  $\alpha_{0,1,2,3}$  are loss weights tuned adaptively by an algorithm called modified gradient normalization (MGN) [46] to ensure that all tasks can be learned at the same pace. To learn semantic segmentation, we use a combination of pixel-wise cross entropy and dice loss as in (6).

$$\mathcal{L}_{SEG} = \left( \frac{1}{N} \sum_{i=1}^N y_i \log(\hat{y}_i) + (1 - y_i) \log(1 - \hat{y}_i) \right) + \left( 1 - \frac{2|\hat{y} \cap y|}{|\hat{y}| + |y|} \right), \quad (6)$$

where  $N$  is the total elements at the last layer of the segmentation decoder, while  $y_i$  and  $\hat{y}_i$  are ground truth and prediction of element  $i$ . Then, we use L1 loss to supervise waypoints prediction as in (7).

$$\mathcal{L}_{WP} = \frac{1}{M} \sum_{i=1}^M |\hat{y}_i - y_i|, \quad (7)$$

where  $M$  is equal to 6 as there are three predicted waypoints that have x,y coordinates for each. Similarly, we use L1 loss to supervise steering and throttle estimation as in (8). However, averaging is not necessary as there is only one element for each output.

$$\mathcal{L}_{\{ST,TH\}} = |\hat{y} - y| \quad (8)$$

Table 2: Model Specification

Model	Total Parameters↓	Model Size ↓	Input/Sensor	Output
Huang et al. [30]	74953258	300.196 MB	RGBD, High-level commands	Segmentation, Steering, Throttle
AIM-MT [23]	27967063	112.078 MB	RGB, GNSS, 9-axis IMU, Rotary encoder	Segmentation, Depth, Waypoints, Steering, Throttle
DeepIPC	20983128	84.972 MB	RGBD, GNSS, 9-axis IMU, Rotary encoder	Segmentation, BEV Semantic, Waypoints, Steering, Throttle

AIM-MT [23] is implemented based on the codes shared in the author’s repository at <https://github.com/autonomousvision/neat>. Meanwhile, Huang et al.’s model [30] is implemented based on the explanation written in the paper. All models are deployed on a laptop powered with NVIDIA GTX 1650 GPU in performing real-world autonomous driving. As the models can run smoothly during evaluation, we believe that calculating their inference speeds is not necessary. However, we assume that a smaller model with less number of parameters is preferred as it does not consume large computation power.

The model is implemented with PyTorch framework [52] and trained on NVIDIA RTX 3090 by Adam optimizer [53] with a decoupled weight decay [54] of 0.001 and a batch size of 8. The initial learning rate is set to 0.0001 and divided by 2 if validation  $\mathcal{L}_{MTL}$  is not dropping in 5 epochs. To avoid unnecessary computation, the training is stopped if there is no improvement in 30 epochs.

### 3.5. Evaluation and Scoring

DeepIPC is evaluated under two conditions with varying cloud intensity with two different tests namely offline and online tests. For each condition, the final score is obtained by averaging the scores from three experimental results. In the offline test, the model is deployed to predict driving records. Then, its performance on each task is calculated by a specific metric function. To evaluate waypoints and navigational controls, we use mean absolute error (MAE) or L1 loss as in (7) and (8). Meanwhile, we compute intersection over union (IoU) as in (9) for evaluating the segmentation performance.

$$IoU_{SEG} = \frac{|\hat{y} \cap y|}{|\hat{y} \cup y|} \quad (9)$$

We define the best model by the lowest total metric (TM) score as formulated with (10) that combines segmentation IoU and controls estimation MAE. Depth and waypoints MAE are excluded since not every model has these outputs.

$$TM = (1 - IoU_{SEG}) + MAE_{ST} + MAE_{TH} \quad (10)$$

In the online test, the model is deployed to drive a robotic vehicle by following a set of routes. Unlike in our previous work [1], the vehicle is prevented from

---

#### Algorithm 2: Route points to Commands

---

```

if  $Rp_1^x \leq -4m$  or  $Rp_2^x \leq -8m$  then
  | command = turn left
else if  $Rp_1^x \geq 4m$  or  $Rp_2^x \geq 8m$  then
  | command = turn right
else
  | command = go straight

```

.....  
 $Rp_{\{1,2\}}^x$ : the route point’s local  $x$  position

---

colliding with other objects as it can cause unnecessary damage. Thus, we determine the drivability score by counting the number and time of interventions needed to prevent collisions.

In addition, we conduct a comparative study with some recent models to get a clearer performance justification. Table 2 shows the specification of the models evaluated in this study where our DeepIPC is considered to be the smallest model as it has the lowest number of parameters. We evaluate a model proposed by Huang et al. [30] that takes RGB images and depth maps but with a different fusion strategy. This model uses high-level commands in selecting a command-specific controller. Hence, we generate these commands automatically based on the route point position in the local coordinate using a certain rule as described in Algorithm 2. We also evaluate AIM-MT [23] which only takes RGB images and predicts multiple vision tasks for extra supervision. By performing more vision tasks, the perception module can provide better features for the controller. For a fair comparison, we modify both models to process the same information as provided to DeepIPC.



Table 3: Multi-task Performance Score

Condition	Model	Total Metric↓	$IoU_{SEG}$ ↑	$MAE_{DE}$ ↓	$MAE_{WP}$ ↓	$MAE_{ST}$ ↓	$MAE_{TH}$ ↓
Noon	Huang et al. [30]	$0.4778 \pm 0.0281$	0.8300	-	-	0.2422	0.0484
	AIM-MT [23]	$0.2932 \pm 0.0300$	0.8863	0.0593	0.0983	0.1734	<b>0.0061</b>
	<b>DeepIPC</b>	<b><math>0.2807 \pm 0.0335</math></b>	<b>0.8899</b>	-	<b>0.0683</b>	<b>0.1632</b>	0.0074
Evening	Huang et al. [30]	$0.4875 \pm 0.0453$	0.7952	-	-	0.2384	0.0443
	AIM-MT [23]	$0.3088 \pm 0.0346$	0.8578	0.0669	0.0931	0.1639	<b>0.0026</b>
	<b>DeepIPC</b>	<b><math>0.3030 \pm 0.0369</math></b>	<b>0.8623</b>	-	<b>0.0645</b>	<b>0.1611</b>	0.0041

The best performance is defined by the lowest total metric score.  $IoU_{SEG}$ : IoU score of semantic segmentation.  $MAE_{DE}$ : mean absolute error of normalized depth estimation.  $MAE_{WP}$ : mean absolute error of waypoints prediction.  $MAE_{ST}$ : mean absolute error of steering estimation.  $MAE_{TH}$ : mean absolute error of throttle estimation.

## 4. Result and Discussion

To understand its intuitive performance, DeepIPC is evaluated using two different methods namely the offline test and the online test. The results can be seen in Table 3 and Table 4 respectively. Meanwhile, the qualitative results are shown in Fig. 5.

### 4.1. Offline Test

The offline test is used to evaluate the model’s performance in handling multiple perception and control tasks simultaneously. All models are deployed to predict driving records and evaluated with multi-task and task-wise scoring. The test dataset is recorded three times in a completely different area from the train-val dataset. Each record is taken on different days to vary the situation and cloud intensity.

Table 3 shows that DeepIPC achieves the best performance by having the lowest total metric score in all conditions. However, all models including DeepIPC have performance degradation in the evening. This means that doing inference in the low light condition is harder than in the normal condition. Specifically, in the segmentation task, DeepIPC has a higher IoU than AIM-MT even though it does not perform depth estimation for extra supervision that can enhance the RGB encoder. Thanks to the end-to-end learning strategy where the segmentation prediction can be processed further through the encoding and decoding process of the BEV semantic map. Therefore, the segmentation decoder receives a more useful gradient signal to tune the network weights properly. Meanwhile, Huang et al.’s model has the

worst segmentation performance which is caused by conflicting features from fusing RGB images and depth maps from the early perception stage.

In the waypoints prediction task, DeepIPC has a lower MAE compared to AIM-MT. Thanks to the BEV semantic features, DeepIPC can distinguish free and occupied areas easily from the top-view perspective. Thus, it can properly estimate the waypoints which are also laid in BEV space. Although AIM-MT predicts four waypoints and DeepIPC only predicts three waypoints, it is still considered a fair comparison because the MAE formula averages the error across all predictions. The reason the AIM-MT predicts four waypoints is to let its controller module have more learning experiences in estimating the waypoints correctly. However, DeepIPC still performs better as its controller module gets boosted by BEV semantic features and fed with angular speed measurement which enhances its intuition. This result is in line with the result in our previous work [1] where the model that perceives in BEV perspective (by using depth projection or LiDAR) is better at estimating the waypoints than the model that perceives in front-view perspective only.

In the navigational controls estimation task, DeepIPC also has the best performance in line with the waypoints prediction result. The MLP agent can leverage useful features encoded from both RGB and BEV semantic maps. Therefore, the MLP agent can perform as well as the PID agent in estimating steering and throttle. With two different agents considering various aspects of driving, more appropriate action can be decided. Compared to AIM-

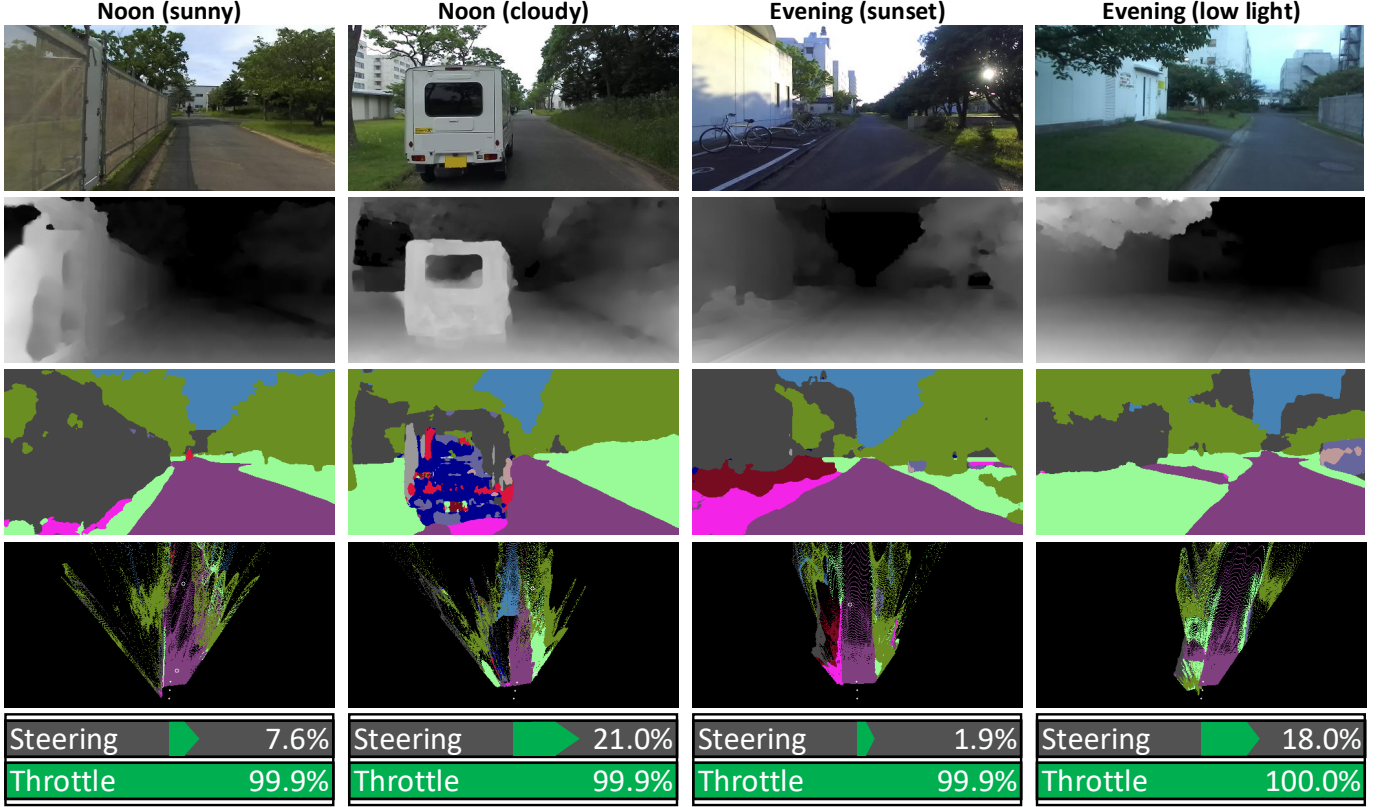


Figure 5: Driving footage. See the driving video at <https://youtu.be/AiKotQ-IAzw> for more details, including failure cases where we intervene in the model to avoid collisions. Sunny noon: DeepIPC makes a small steering adjustment to the right as the vehicle is too close to the terrain. Cloudy noon: Although DeepIPC cannot segment the car properly, it can avoid collision as it knows that the left side is occupied. Sunset evening: DeepIPC makes a small steering adjustment to keep on its lane. Low light evening: We intervene in DeepIPC to avoid driving off-road on the vegetation as it keeps the throttle maximum and fails to make a right turn.

Table 4: Drivability Score

Condition	Model	Intervention↓	
		Count	Time (secs)
Noon	Huang et al. [30]	$1.8889 \pm 0.4157$	$5.6039 \pm 1.7272$
	AIM-MT [23]	$2.2778 \pm 0.3425$	$4.2161 \pm 0.8380$
	<b>DeepIPC</b>	<b><math>1.1111 \pm 0.3928</math></b>	<b><math>2.3092 \pm 0.9841</math></b>
Evening	<b>Huang et al. [30]</b>	<b><math>1.6111 \pm 0.2079</math></b>	$4.5532 \pm 0.2160$
	AIM-MT [23]	$2.6667 \pm 0.1361$	$4.6736 \pm 0.4293$
	<b>DeepIPC</b>	$1.8889 \pm 0.3928$	<b><math>4.2286 \pm 0.6102</math></b>

The best drivability is defined by the lowest intervention.

MT, DeepIPC is better at estimating the steering but worse at estimating the throttle. Yet, it can be said that DeepIPC is better than AIM-MT considering that better steering is more important than better throttle in low-speed driving. Meanwhile, Huang et al.’s model performs the worst as its controller module gets stuck with certain behavior. Be noted that the offline test results can be different from the online test results. This is because any predictions will not affect the next states as they are prerecorded.

#### 4.2. Online Test

The purpose of the online test is to evaluate the model’s drivability in driving the vehicle. The model must drive the vehicle safely by following a set of route points while avoiding obstacles (e.g., a vehicle stopped on the left side of the road). The experiment is conducted three times for each condition and on different days to vary the situations. The performance is evaluated based on the average intervention count and intervention time. The less the driver does intervention means the better the driving performance. For a fair comparison, the experiments for all models are monitored by the same driver in preventing a collision. Thus, each intervention is based on the same perspective of the degree of danger. Some driving records can be seen in Fig. 5.

Table 4 shows that DeepIPC achieves the best drivability at noon where it has the lowest intervention count and intervention time. Meanwhile, DeepIPC is comparable to Huang et al.’s model in the evening

where it achieves the lowest intervention time but has a higher intervention count. Keep in mind that a model with a lower intervention count can have a longer intervention time. For example, a model that fails to make a turn and going to collide needs more correction time than a model that makes a small deviation on a straight path. Hence, it depends on the degree of danger in which the collision is going to happen. Based on the intervention time per intervention count, it is obvious that Huang et al.'s model needs more correction time for each intervention which means that it has the highest danger level compared to DeepIPC and AIM-MT.

Furthermore, in a comparison of drivability in the evening, DeepIPC and AIM-MT perform worse than Huang et al.'s model. In line with the offline result, the model that mainly takes RGB images failed to perceive the environment in the evening as the provided image is not as clearly visible as when driving at noon. On the contrary, Huang et al.'s model become better as it can leverage the information from the depth map that is concatenated with the RGB image from the beginning of the perception phase. This means that although the early fusion strategy causes conflicting features for semantic segmentation, it is useful for driving in low-light conditions. Moreover, even though Huang et al.'s model shows inferior performance on navigational controls estimation in the offline test, its drivability can be said good enough for performing real-world automated driving in the evening with lower traffic compared when driving at noon. Regardless of its comparable performance with DeepIPC in the evening, this exposes the limitation of imitation learning for a model that purely relies on human behavior (by directly predicting steering and throttle levels) without considering another driving aspect that can be obtained from predicting future trajectories in the form of waypoints location in the local coordinate.

## 5. Conclusion

We present DeepIPC, an end-to-end model that can drive a vehicle in real environments. The model is evaluated by predicting driving records and performing automated driving. Furthermore, a comparative study is conducted to justify its performance.

Based on the experimental results, we disclosed several findings as follows. First, in line with our previous work [1], the BEV semantic feature is proven can improve the model performance in predicting waypoints and navigational controls. With a better perception, the model can leverage useful information which results in better drivability. Second, driving in the low light condition is harder than in the normal condition, especially for DeepIPC and AIM-MT which only rely on RGB images at the early perception stage. Meanwhile, Huang et al.'s model can tackle this issue as it fuses RGB and depth features earlier. Third, considering its performance and the number of parameters in its architecture, DeepIPC can be said as the best model. Lastly, we also validate that the end-to-end imitation learning method is also effective for a complex multi-input multi-output model that is deployed for performing real-world autonomous driving.

As for future works, the perception module can be enhanced with a LiDAR sensor to handle poor illumination conditions such as driving at night. Then, conducting more evaluations on different areas and adversarial situations (e.g., avoiding collision with pedestrians that cross the street suddenly) is suitable to test the drivability further.

## References

- [1] O. Natan, J. Miura, End-to-end autonomous driving with semantic depth cloud mapping and multi-agent, *IEEE Trans. Intell. Veh.* 8 (1) (2022) 557–571.
- [2] L. Le Mero, D. Yi, M. Dianati, A. Mouzakitis, A survey on imitation learning techniques for end-to-end autonomous vehicles, *IEEE Trans. Intell. Transp. Syst.* 23 (9) (2022) 14128–14147.
- [3] S. Moten, F. Celiberti, M. Grottoli, A. van der Heide, Y. Lemmens, X-in-the-loop advanced driving simulation platform for the design, development, testing and validation of ADAS, in: *Proc. IEEE Intell. Veh. Symp. (IV)*, Changshu, China, 2018, pp. 1–6.
- [4] T. Wu, A. Luo, R. Huang, H. Cheng, Y. Zhao, End-to-end driving model for steering control of autonomous vehicles with future spatiotemporal features, in: *Proc. IEEE/RSJ Inter. Conf. Intell. Robots and Syst. (IROS)*, Macau, China, 2019, pp. 950–955.
- [5] D. Omeiza, H. Web, M. Jirotko, L. Kunze, Towards accountability: Providing intelligible explanations in autonomous driving, in: *Proc. IEEE Intell. Veh. Symp. (IV)*, Nagoya, Japan, 2021, pp. 231–237.

- [6] D. Feng, C. Haase-Schütz, L. Rosenbaum, H. Hertlein, C. Gläser, F. Timm, W. Wiesbeck, K. Dietmayer, Deep multi-modal object detection and semantic segmentation for autonomous driving: Datasets, methods, and challenges, *IEEE Trans. Intell. Transp. Syst.* 22 (3) (2021) 1341–1360.
- [7] M. Teti, W. E. Hahn, S. Martin, C. Teti, E. Barenholtz, A controlled investigation of behaviorally-cloned deep neural network behaviors in an autonomous steering task, *Robotics and Autonomous Systems* 142 (2021) 103780.
- [8] A. Amini, I. Gilitschenski, J. Phillips, J. Moseyko, R. Banerjee, S. Karaman, D. Rus, Learning robust control policies for end-to-end autonomous driving from data-driven simulation, *IEEE Robot. and Autom. Lett.* 5 (2) (2020) 1143–1150.
- [9] A. Ngo, M. P. Bauer, M. Resch, A multi-layered approach for measuring the simulation-to-reality gap of radar perception for autonomous driving, in: *Proc. IEEE Intell. Transp. Syst. Conf. (ITSC)*, Indianapolis, USA, 2021, pp. 4008–4014.
- [10] J. Zhou, R. Wang, X. Liu, Y. Jiang, S. Jiang, J. Tao, J. Miao, S. Song, Exploring imitation learning for autonomous driving with feedback synthesizer and differentiable rasterization, in: *Proc. IEEE/RSJ Inter. Conf. Intell. Robots and Syst. (IROS)*, Prague, Czech Republic, 2021, pp. 1450–1457.
- [11] J. Hawke, R. Shen, C. Gurau, S. Sharma, D. Reda, N. Nikolov, P. Mazur, S. Micklethwaite, N. Griffiths, A. Shah, A. Kendall, Urban driving with conditional imitation learning, in: *Proc. IEEE Inter. Conf. Robot. and Autom. (ICRA)*, Paris, France, 2020, pp. 251–257.
- [12] B. D. Argall, S. Chernova, M. Veloso, B. Browning, A survey of robot learning from demonstration, *Robotics and Autonomous Systems* 57 (5) (2009) 469–483.
- [13] D. Xu, Z. Ding, X. He, H. Zhao, M. Moze, F. Aioun, F. Guillemand, Learning from naturalistic driving data for human-like autonomous highway driving, *IEEE Trans. Intell. Transp. Syst.* 22 (12) (2021) 7341–7354.
- [14] H. Ma, Y. Wang, R. Xiong, S. Kodagoda, L. Tang, DeepGoal: Learning to drive with driving intention from human control demonstration, *Robotics and Autonomous Systems* 127 (2020) 103477.
- [15] B. Ranft, C. Stiller, The role of machine vision for intelligent vehicles, *IEEE Trans. Intell. Veh.* 1 (1) (2016) 8–19.
- [16] S. Matsuzaki, J. Miura, H. Masuzawa, Multi-source pseudo-label learning of semantic segmentation for the scene recognition of agricultural mobile robots, *Advanced Robotics* 36 (19) (2022) 1011–1029.
- [17] H. Masuzawa, J. Miura, Image-based recognition of green perilla leaves using a deep neural network for robotic harvest support, *Advanced Robotics* 35 (6) (2021) 359–367.
- [18] M. Hahner, D. Dai, C. Sakaridis, J.-N. Zaeche, L. V. Gool, Semantic understanding of foggy scenes with purely synthetic data, in: *Proc. IEEE Intell. Transp. Syst. Conf. (ITSC)*, Auckland, New Zealand, 2019, pp. 3675–3681.
- [19] R. N. Rajaram, E. Ohn-Bar, M. M. Trivedi, RefineNet: Refining object detectors for autonomous driving, *IEEE Trans. Intell. Veh.* 1 (4) (2016) 358–368.
- [20] J. Wang, X. Wang, T. Shen, Y. Wang, L. Li, Y. Tian, H. Yu, L. Chen, J. Xin, X. Wu, N. Zheng, F.-Y. Wang, Parallel vision for long-tail regularization: Initial results from IVFC autonomous driving testing, *IEEE Trans. Intell. Veh.* 7 (2) (2022) 286–299.
- [21] J. Yoo, R. Langari, A predictive perception model and control strategy for collision-free autonomous driving, *IEEE Trans. Intell. Transp. Syst.* 20 (11) (2019) 4078–4091.
- [22] K. Ishihara, A. Kanervisto, J. Miura, V. Hautamaki, Multi-task learning with attention for end-to-end autonomous driving, in: *Proc. IEEE/CVF Conf. Comput. Vision and Pattern Recog. Workshops (CVPRW)*, Nashville, USA, 2021, pp. 2896–2905.
- [23] K. Chitta, A. Prakash, A. Geiger, NEAT: Neural attention fields for end-to-end autonomous driving, in: *Proc. IEEE/CVF Inter. Conf. Comput. Vision (ICCV)*, Montreal, Canada, 2021, pp. 15773–15783.
- [24] O. Natan, J. Miura, Semantic segmentation and depth estimation with RGB and DVS sensor fusion for multi-view driving perception, in: *Proc. Asian Conf. Pattern Recog. (ACPR)*, Jeju Island, South Korea, 2021, pp. 352–365.
- [25] T. Suzuki, K. Ohno, S. Kojima, N. Miyamoto, T. Suzuki, T. Komatsu, Y. Shibata, K. Asano, K. Nagatani, Estimation of articulated angle in six-wheeled dump trucks using multiple gnss receivers for autonomous driving, *Advanced Robotics* 35 (23) (2021) 1376–1387.
- [26] A. Prakash, K. Chitta, A. Geiger, Multi-modal fusion transformer for end-to-end autonomous driving, in: *Proc. IEEE/CVF Conf. Comput. Vision and Pattern Recog. (CVPR)*, Nashville, USA, 2021, pp. 7073–7083.
- [27] K. Chitta, A. Prakash, B. Jaeger, Z. Yu, K. Renz, A. Geiger, TransFuser: Imitation with transformer-based sensor fusion for autonomous driving, *IEEE Trans. Pattern Anal. Mach. Intell.* (2022).
- [28] U. Niesen, J. Unnikrishnan, Camera-radar fusion for 3-D depth reconstruction, in: *Proc. IEEE Intell. Veh. Symp. (IV)*, Las Vegas, USA, 2020, pp. 265–271.
- [29] M. Shan, Y. Zou, M. Guan, C. Wen, C.-L. Ng, A leader-following approach based on probabilistic trajectory estimation and virtual train model, in: *Proc. IEEE Intell. Transp. Syst. Conf. (ITSC)*, Yokohama, Japan, 2017, pp. 1–6.
- [30] Z. Huang, C. Lv, Y. Xing, J. Wu, Multi-modal sensor fusion-based deep neural network for end-to-end autonomous driving with scene understanding, *IEEE Sensors J.* 21 (10) (2021) 11781–11790.
- [31] F. Sasaki, T. Yohira, A. Kawaguchi, Adversarial behavioral cloning, *Advanced Robotics* 34 (9) (2020) 592–598.
- [32] H. Shen, W. Wan, H. Wang, Learning category-level generalizable object manipulation policy via generative adversarial self-imitation learning from demonstrations, *IEEE Robot. and Autom. Lett.* 7 (4) (2022) 11166–11173.
- [33] D.-T. Pham, T.-N. Tran, S. Alam, V. N. Duong, A gener-

- ative adversarial imitation learning approach for realistic aircraft taxi-speed modeling, *IEEE Trans. Intell. Transp. Syst.* 23 (3) (2022) 2509–2522.
- [34] X. Fang, Q. Zhang, Y. Gao, D. Zhao, Offline reinforcement learning for autonomous driving with real world driving data, in: *Proc. IEEE Intell. Transp. Syst. Conf. (ITSC)*, Macau, China, 2022, pp. 3417–3422.
- [35] R. Bhattacharyya, B. Wulfe, D. J. Phillips, A. Kuefler, J. Morton, R. Senanayake, M. J. Kochenderfer, Modeling human driving behavior through generative adversarial imitation learning, *IEEE Trans. Intell. Transp. Syst.* 24 (3) (2023) 2874–2887.
- [36] P. Cai, H. Wang, H. Huang, Y. Liu, M. Liu, Vision-based autonomous car racing using deep imitative reinforcement learning, *IEEE Robot. and Autom. Lett.* 6 (4) (2021) 7262–7269.
- [37] A. Chatty, P. Gaussier, S. K. Hasnain, I. Kallel, A. M. Alimi, The effect of learning by imitation on a multi-robot system based on the coupling of low-level imitation strategy and online learning for cognitive map building, *Advanced Robotics* 28 (11) (2014) 731–743.
- [38] S. Hoshino, K. Unuma, End-to-end motion planners through multi-task learning for mobile robots with 2D lidar, in: *Proc. IEEE/SICE Inter. Symp. Syst. Integration (SII)*, Atlanta, USA, 2023, pp. 1–6.
- [39] S. Yan, Z. Wu, J. Wang, Y. Huang, M. Tan, J. Yu, Real-world learning control for autonomous exploration of a biomimetic robotic shark, *IEEE Trans. Ind. Electron.* 70 (4) (2023) 3966–3974.
- [40] O. Natan, D. U. K. Putri, A. Dharmawan, Deep learning-based weld spot segmentation using modified UNet with various convolutional blocks, *ICIC Express Lett. Part B: Applications* 12 (12) (2021) 1169–1176.
- [41] R. Araki, T. Hirakawa, T. Yamashita, H. Fujiyoshi, MT-DSSD: Multi-task deconvolutional single shot detector for object detection, segmentation, and grasping detection, *Advanced Robotics* 36 (8) (2022) 373–387.
- [42] M. Tan, Q. Le, EfficientNet: Rethinking model scaling for convolutional neural networks, in: *Proc. Inter. Conf. Machine Learning (ICML)*, Long Beach, USA, 2019, pp. 6105–6114.
- [43] S. Ioffe, C. Szegedy, Batch normalization: Accelerating deep network training by reducing internal covariate shift, in: *Proc. Inter. Conf. Machine Learning (ICML)*, Lille, France, 2015, pp. 448–456.
- [44] V. Nair, G. E. Hinton, Rectified linear units improve restricted boltzmann machines, in: *Proc. Inter. Conf. Machine Learning (ICML)*, Haifa, Israel, 2010, pp. 807–814.
- [45] K. Cho, B. van Merriënboer, D. Bahdanau, Y. Bengio, On the properties of neural machine translation: Encoder-decoder approaches, in: *Proc. Workshop Syntax, Semantics and Structure in Statistical Translation (SSST)*, Doha, Qatar, 2014, pp. 103–111.
- [46] O. Natan, J. Miura, Towards compact autonomous driving perception with balanced learning and multi-sensor fusion, *IEEE Trans. Intell. Transp. Syst.* 23 (9) (2022) 16249–16266.
- [47] A. O. Ly, M. Akhloufi, Learning to drive by imitation: An overview of deep behavior cloning methods, *IEEE Trans. Intell. Veh.* 6 (2) (2021) 195–209.
- [48] G. A. G. Ricardez, N. Koganti, P.-C. Yang, S. Okada, P. M. U. Eljuri, A. Yasuda, L. E. Hafi, M. Yamamoto, J. Takamatsu, T. Ogasawara, Adaptive motion generation using imitation learning and highly compliant end effector for autonomous cleaning, *Advanced Robotics* 34 (3-4) (2020) 189–201.
- [49] H. Fujiishi, T. Kobayashi, K. Sugimoto, Safe and efficient imitation learning by clarification of experienced latent space, *Advanced Robotics* 35 (16) (2021) 1012–1027.
- [50] E. Xie, W. Wang, Z. Yu, A. Anandkumar, J. M. Alvarez, P. Luo, SegFormer: Simple and efficient design for semantic segmentation with transformers, in: *Proc. Inter. Conf. Neural Information Processing Syst. (NIPS)*, Online, 2021, pp. 1–18.
- [51] M. Cordts, M. Omran, S. Ramos, T. Rehfeld, M. Enzweiler, R. Benenson, U. Franke, S. Roth, B. Schiele, The cityscapes dataset for semantic urban scene understanding, in: *Proc. IEEE/CVF Conference on Comput. Vision and Pattern Recog. (CVPR)*, Las Vegas, USA, 2016, pp. 3213–3223.
- [52] A. Paszke, S. Gross, F. Massa, A. Lerer, J. Bradbury, G. Chanan, T. Killeen, Z. Lin, N. Gimelshein, L. Antiga, A. Desmaison, A. Kopf, E. Yang, Z. DeVito, M. Raison, A. Tejani, S. Chilamkurthy, B. Steiner, L. Fang, J. Bai, S. Chintala, PyTorch: An imperative style, high performance deep learning library, in: *Proc. Inter. Conf. Neural Information Processing Syst. (NIPS)*, Vancouver, Canada, 2019, pp. 8024–8035.
- [53] D. P. Kingma, J. Ba, Adam: A method for stochastic optimization, in: *Proc. Inter. Conf. Learning Representations (ICLR)*, San Diego, USA, 2015, pp. 1–15.
- [54] I. Loshchilov, F. Hutter, Decoupled weight decay regularization, in: *Proc. Inter. Conf. Learning Representations (ICLR)*, New Orleans, USA, 2019, pp. 1–10.